

# Two-dimensional Offsets via Medial Axis Transform II: Algorithm\*

Hyeong In Choi, Chang Yong Han

School of Mathematics, Seoul National University

Sung Woo Choi

Max-Planck-Institut für Informatik

Hwan Pyo Moon<sup>†</sup>

Research Institute of Mathematics,  
Seoul National University

Kyeong Hah Roh

Graduate School of Education, Ewha Womans University

Nam-Sook Wee<sup>‡</sup>

Department of Industrial Engineering, Hansung University

## Abstract

This paper is the second half of the two-part installment of the result dealing with the two-dimensional offset curves by utilizing the medial axis transform. We present an algorithm for the offset curve computation of a planar domain whose boundary is composed of rational curve segments. All such offset algorithms involve the two-stage process: the computation of offsets to each curve segments and the decision of valid portions of each offset curve segment. Since there are plenty of literature regarding the first issue, we primarily focus on

---

\*Supported in part by KOSEF-102-07-2, SNU-RIM, and BK21 program.

<sup>†</sup>Supported in part by NSF(CCR-9902669) at the University of California, Davis.

<sup>‡</sup>Supported by research fund from Hansung University.

the second issue here. Most known methods dealing with the second process involve a step of computing curve/curve intersection, which in some cases cause numerical errors that may cause subtle topological difficulties. Our method proposed here differs in its basic principle. It advocates the philosophy that once the domain is decomposed in a suitable way the medial axis transform can be fully utilized to provide a numerically stable algorithm. Furthermore, this algorithm is designed in such a way that the topological feature is handled in a localized manner. In fact, this localization procedure enables one to isolate any problem areas, be they numerical or topological. The basic strategy of our localization procedure is to break up the domain into many subdomains each of whose medial axis transform has a *monotone* increasing/decreasing radius component. In these subdomains, the problem reduces to that of root finding, where we can apply any numerical schemes such as the Newton-Raphson method. The concept of monotonicity plays a key role in enhancing the stability of the algorithm. One of the novelty of this paper is the way it is systematically incorporated in the algorithms. Once we locate the self-intersection points and construct the offset curves of the subdomains, we can link them together to form the offset curve of the whole domain by following the principle of domain decomposition.

## 1 Introduction

The offset curve we consider in this paper is the inner offset curve of a planar domain which can be multiply connected and whose boundary is composed of piecewise rational curves.

One of the problems when dealing with this kind of offset curve is that a rational curve  $\mathbf{r}(t) = (x(t), y(t))$  does not allow in general a rational offset curve. In contrast to a polygon and an arc, the untrimmed  $d$ -offset curve

$$\mathbf{r}_d(t) = \mathbf{r}(t) + d \frac{(-y'(t), x'(t))}{\sqrt{x'(t)^2 + y'(t)^2}}, \quad (1)$$

which is at a  $d$  distance away from  $\mathbf{r}(t)$ , is not in general rational. (Here we chose one of the two possible offset curves of  $\mathbf{r}(t)$  such that  $\mathbf{r}_d(t)$  is on the left side of  $\mathbf{r}(t)$  as we traverse  $\mathbf{r}(t)$  in the direction of increasing  $t$ .)

This is, of course, the consequence of the term  $\sqrt{x'(t)^2 + y'(t)^2}$ . Thus,  $\mathbf{r}_d(t)$  can be a rational curve if and only if

$$x'(t)^2 + y'(t)^2 = \sigma(t)^2 \quad (2)$$

for some rational function  $\sigma(t)$ . Those curves satisfying Equation (2) are called Pythagorean hodograph curves. They are introduced by Farouki and

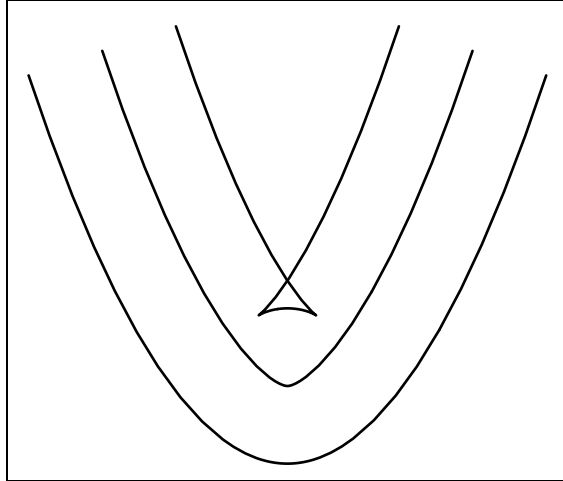


Figure 1: A fish tail

Sakkalis [15], and have a rational expression for their offset curves. In general, however, a rational curve  $\mathbf{r}(t)$  is not a Pythagorean hodograph curve. So, we cannot expect a rational expression for  $\mathbf{r}_d(t)$ , and the best job we can do may be generating a finite sequence of points lying on  $\mathbf{r}_d(t)$  as accurately as possible, and then interpolating these points such that the interpolant  $\tilde{\mathbf{r}}_d(t)$  is within the given error tolerance with respect to  $\mathbf{r}_d(t)$ .

Another and yet tougher problem arises as  $d$  increases. For some large  $d$ , the untrimmed offset curve  $\mathbf{r}_d(t)$  given by Formula (1) is no longer the true  $d$ -offset curve of  $\mathbf{r}(t)$ . See Figure 1. This kind of phenomena happens when the offset distance  $d$  is too large compared to the radius of curvature of  $\mathbf{r}(t)$ . Especially, the cusps of  $\mathbf{r}_d(t)$  lie on the evolute  $\mathbf{e}(t)$  of  $\mathbf{r}(t)$  defined by

$$\mathbf{e}(t) = \mathbf{r}(t) + \frac{1}{\kappa(t)}\mathbf{n}(t),$$

where  $\kappa(t)$  is the (signed) curvature of  $\mathbf{r}(t)$ . See [12]. Now if  $d > 1/\kappa(t) > 0$  for some  $t$ , then  $\mathbf{r}_d(t)$  may interfere with itself, forming a self-intersection point. To get the true  $d$ -offset curve of  $\mathbf{r}(t)$ , we need to remove the “fish-tail” portion.

The untrimmed offset curve  $\mathbf{r}_d(t)$  may intersect itself even if  $\kappa(t) < 0$ . This happens when the domain is too “narrow” compared with the offset distance  $d$ . See Figure 2. This kind of self-intersection is not due to the local geometry of the boundary curve as in the fish-tail case, but due to the global shape of the domain. But in this case too, we can obtain the true  $d$ -offset curve by deleting the segments defined by two self-intersection points.

Hence, we must have a method for identifying self-intersection points. If

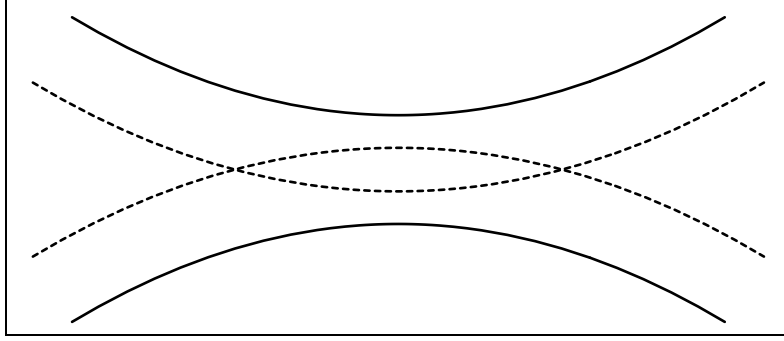


Figure 2: A narrow domain (partial view)

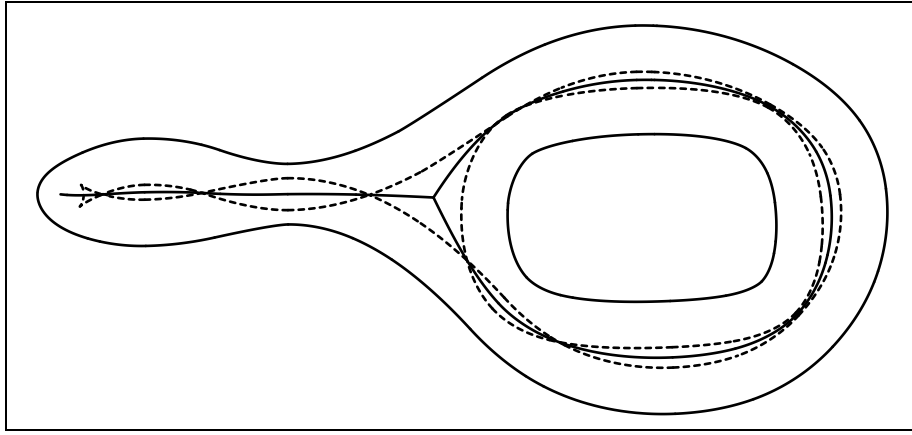


Figure 3: A medial axis and self-intersection points

the boundary curve consists of polygons and arcs, this is not a hard problem since all we have to compute are the intersections of pairs of line and line, line and arc, and arc and arc. But with a generic piecewise rational boundary curve, the computation is not so simple. In fact, Farouki and Neff [11] have shown that this computation amounts to solving very high-degree algebraic equations.

Self-intersection points are closely related to the medial axis or the medial axis transform. For each self-intersection point  $\mathbf{p}$  of a  $d$ -offset curve, there are two corresponding foot points  $\mathbf{q}_1$  and  $\mathbf{q}_2$  on the boundary curve such that  $|\overline{\mathbf{p}\mathbf{q}_1}| = |\overline{\mathbf{p}\mathbf{q}_2}|$ . Thus the circle centered at  $\mathbf{p}$  with radius  $r = |\overline{\mathbf{p}\mathbf{q}_1}|$  is maximally inscribed in the domain. That is,  $\mathbf{p}$ , the self-intersection point, is also a medial axis point. In Figure 3, we can see that the medial axis passes through all the self-intersection points. In fact, all the self-intersection points of  $\mathbf{r}_d(t)$  exactly correspond to the medial axis transform points with a  $d$  radius component.

Although the medial axis transform cannot be expressed in a closed-form using the parameter of the boundary curve, we have seen its geometric nature; the medial axis transform is a geometric graph. (See [4].) A geometric graph is a usual graph with real analytic curves as edges. Being a geometric graph has two implications to the algorithm for computing the medial axis transform. Firstly, the points of the medial axis transform we successively find can be organized into a graph data structure (actually, a tree data structure thanks to the homology-killing process). Secondly, each real analytic edge can be approximated as accurately as possible by a Bézier curve. In doing so, a divide-and-conquer strategy, called domain decomposition, is the basis of the algorithm, which decomposes a complex domain into many simple and easy to handle subdomains. In this way we can extract the medial axis transform from a domain with high accuracy. For more detail, one can refer to [5].

On the other hand, we clarified the relation between the medial axis transform and offset curves in the preceding paper. It says that the  $d$ -offset curve of a domain can be recovered (using the envelope formula) from the  $d$ -cutoff of the domain's medial axis transform, where the  $d$ -cutoff is a result of a simple operation which pulls down the medial axis transform to the negative  $z$ -direction by  $d$  and removes what is below the  $xy$ -plane. By using the relation we thoroughly examined the geometry of offset curves.

Armed with the medial axis transform, and bearing in mind its relation with the offset curves, we can now tackle the problem of offset computation. This will be carried out in the following order. Roughly speaking, our goal is to chop the domain into such simple pieces that it is straightforward to compute the offset curve of each piece. Firstly, we will review the basic definitions and key properties of the medial axis transform, for example, the geometric graph and the domain decomposition lemma. Secondly, an algorithm for locating some special points of the medial axis transform will be discussed. These are the horizontal sections of the preceding paper with critical radius values. After identifying the critical horizontal sections, we have our domain decomposed into many fundamental domains whose medial axis transform have a monotone increasing/decreasing radius function component. Then, it is simple to compute the offset curve of this kind of fundamental domain, which is the content of Section 4. Finally, we will discuss the error of the computed offset curve and conclude with some illustrative examples.

## 2 Domain decomposition revisited

Although the medial axis transform does not allow in general any closed-form expression via the parameterization of the boundary, one can find the contact disk corresponding to any boundary points. In [5] and [14], algorithms are presented to pinpoint the medial axis transform point  $(\mathbf{p}, r)$  corresponding to a given boundary point  $\mathbf{q}$ . The first one draws a suspect disk contacting the boundary curve at  $\mathbf{q}$  and intersecting the other boundary curve, and then reduce this disk until it is tangent to the other boundary curve. On the other hand, the second one, called curve/curve-bisector, is based on the observation that  $\mathbf{p}$  is the intersection point of the normal line of the boundary curve at  $\mathbf{q}$  and the point/curve bisector of  $\mathbf{q}$  and the other boundary curve. These algorithms are the workhorse of our algorithm and we will call them, in a general term, the medial axis transform engines.

The medial axis transform can be approximated by interpolating the points found by the medial axis transform engines. The very property of the medial axis transform that makes this process possible is that they are one-dimensional objects composed of a finite number of real analytic curves. We can clarify this idea by saying the medial axis transform is a geometric graph. We call a set in  $\mathbb{R}^3$  a geometric graph, if it is topologically a usual connected graph with a finite number of vertices and edges, where a vertex is a point in or  $\mathbb{R}^3$  and an edge is a real analytic curve with finite length whose limits of tangents at the end points exist. (The same holds for the medial axis in  $\mathbb{R}^2$ .)

If we have an approximation of the medial axis transform, we can figure out the shape of a domain since the medial axis transform is a strong deformation retract of the domain. To get a more accurate approximation of the medial axis transform, we find more contact disks using the medial axis transform engines, and include them in the interpolation scheme. Now, when we run the medial axis transform engines to find those additional contact disks, we don't have to consider the whole domain. All we need to consider is the region around such contact disks. For example if we want to find a medial axis point  $\mathbf{p}$  in Figure 4, we can concentrate our attention on the shaded region only, not the whole domain. This is the idea of the domain decomposition.

**Theorem 1 (Domain Decomposition Lemma).** *For any fixed medial axis point  $\mathbf{p} \in \mathbf{MA}(\Omega)$ , let  $B_r(\mathbf{p})$  be the corresponding contact disk. Suppose  $A_1, \dots, A_m$  are the connected components of  $\Omega \setminus B_r(\mathbf{p})$ . Denote  $\Omega_i = A_i \cup$*

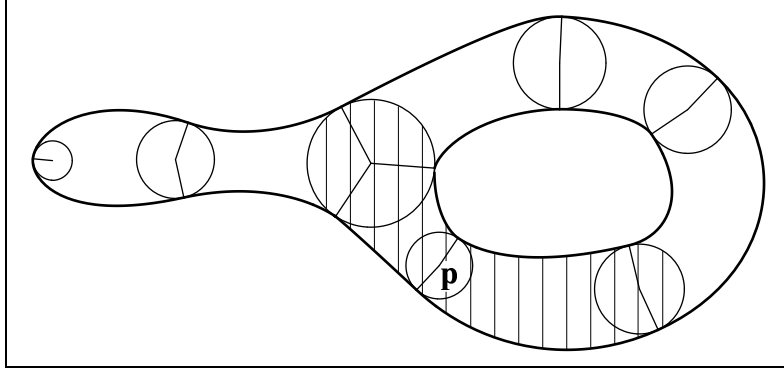


Figure 4: A subdomain around  $\mathbf{p}$

$B_r(\mathbf{p})$  for  $i = 1, \dots, m$ . Then

$$\begin{aligned} \mathbf{MA}(\Omega) &= \bigcup_{i=1}^m \mathbf{MA}(\Omega_i) \quad \text{and} \\ \mathbf{MAT}(\Omega) &= \bigcup_{i=1}^m \mathbf{MAT}(\Omega_i). \end{aligned}$$

Moreover, we have

$$\begin{aligned} \mathbf{MA}(\Omega_i) \cap \mathbf{MA}(\Omega_j) &= \{\mathbf{p}\} \quad \text{and} \\ \mathbf{MAT}(\Omega_i) \cap \mathbf{MAT}(\Omega_j) &= \{(\mathbf{p}, r)\} \end{aligned}$$

for every distinct  $i$  and  $j$ .

Thus, each contact disk decomposes the domain into subdomains. Especially, if we find all the bifurcation points (where at least three edges meet) of the medial axis transform, then the original domains are decomposed into subdomains whose medial axis transforms are piecewise real analytic curves. We call such a subdomain a fundamental domain and the above theorem tells us that it is sufficient to deal with fundamental domains only.

The idea of domain decomposition is also the cornerstone of our offset algorithm. We have seen in [3] that once we construct the offset curves of the original boundary curve segments in fundamental domains, then domain decomposition takes care of how to link them into the whole offset curve of the domain. In Figure 5, for example, we can see that the offset curve of each subdomain does not interfere with other subdomain's offset curve, but can be easily linked with each other, forming the offset curve of the whole domain.

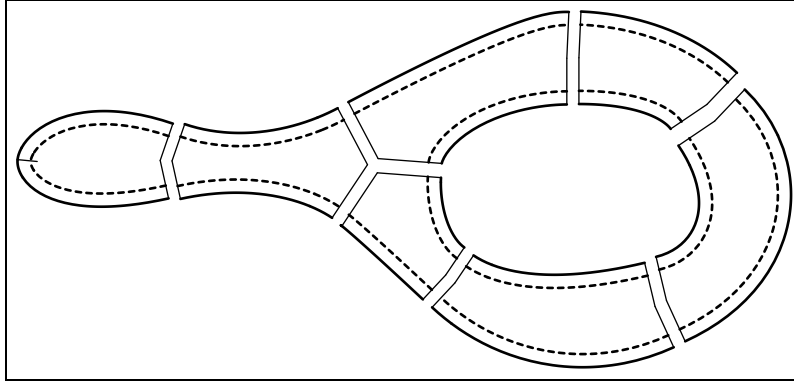


Figure 5: Domain decomposition for offset curves

By the way, the self-intersection points of the  $d$ -offset curve fall on the medial axis where its radius is  $d$ . As we have seen in [3], the set of all medial axis transform points whose radius component is  $c$ , for a given  $c > 0$ , are composed of finite number of points or piecewise  $C^1$  curves. We call a component of this set a  $c$ -horizontal section. The various geometry of  $c$ -horizontal section and the offset curve near self-intersection points is thoroughly discussed in [3]. Hence, it is very important to locate  $d$ -horizontal section to capture the exact nature of  $d$ -offset curve.

However, given a fundamental domain  $\Omega_F$  and  $d > 0$ , locating such  $d$ -horizontal section in  $\Omega_F$  is by no means an easy task. If we assume that  $\mathbf{MAT}(\Omega_F)$  is represented by a piecewise real analytic curve  $(\mathbf{p}(t), r(t))$ , the problem is equivalent to solve the equation  $r(t) = d$ . But we don't have any closed form expression for the function  $r(t)$ . What we have at hand is some engines that compute the value of  $\mathbf{p}(t)$  and  $r(t)$  for given  $t$ . To incorporate such engines into a stable root-finding schemes, one must carefully examine the problem space beforehand.

Thus for the preparation, we are going to further decompose the domain such that the medial axis transform of each subdomain has monotone increasing/decreasing radius component. Once this is done, the solution of the equation  $r(t) = d$  can be efficiently and stably obtained by any traditional numerical methods such as Newton-Raphson method. Thus, special  $c$ -horizontal section which has locally maximum or minimum radius value, which are called *peak* or *valley* respectively, needed to be located in advance. To do so, we use iterative algorithms to *approximately* locate peaks and valleys. As long as we know in advance that there are no other peaks or valleys nearby, these iterative algorithms work well. The trouble occurs when there are other, sometimes infinite, peaks and valleys nearby. One has to have a way of roughly counting these. This can be done by looking at the boundary

geometry. In particular, it is advantageous to decompose the domain such that each of the boundary curve segments of subdomains whose curvature does not change sign.

In doing so, one can also encounter the situation where there are infinitely many peaks or valleys. Since the medial axis transform of our domain is a real analytic curve, infinitely many peaks or valleys occur only when the fundamental domain is *parallel*, this is, the two boundary curve segments are offset to each other. Using Bezout's theorem we will provide an algorithm to determine whether a given domain is parallel.

Now the following section will deal with how to decompose the domain into subdomains whose medial axis transform have monotone radius components, then in Section 4 we can easily compute the points satisfying the equation  $r(t) = d$ .

### 3 Critical horizontal sections

We now discuss how to locate horizontal sections with a critical radius value. Such horizontal sections will be shortly called *critical horizontal sections*. Peaks and valleys are kinds of horizontal sections.

We begin with fixing some conventions on the boundary which will be used throughout this discussion. We assume every curve segment  $\mathbf{r}(t)$  composing the boundary is positively oriented. That is, the parameter  $t$  is so chosen that if one is going along the curve in the direction of increasing  $t$ , then the domain remains to the left.

Let  $\Omega_F$  be a fundamental domain at hand and  $\mathbf{r}$  and  $\mathbf{s}$  be its two boundary curves of the domain defined on the interval  $[0, 1]$ . Let  $\mathbf{p}(t)$  be the corresponding medial axis point of  $\mathbf{r}(t)$ , and let  $\mathbf{s}(u)$  be the foot point of  $\mathbf{p}(t)$  on  $\mathbf{s}$ . The opening angle  $\theta(t)$  of  $\mathbf{p}(t)$  (or  $\mathbf{r}(t)$ ) is the angle from  $\overrightarrow{\mathbf{p}(t)\mathbf{r}(t)}$  to  $\overrightarrow{\mathbf{p}(t)\mathbf{s}(u)}$  in the counterclockwise direction. See Figure 6. If  $\mathbf{p}(t)$  is on a critical horizontal section, then  $\theta(t) = \pi$  since we know that

$$\cos \frac{\theta(t)}{2} = -\tan \phi(t) \tag{3}$$

where  $\phi(t)$  is the angle between the tangent vectors  $(\mathbf{p}'(t), r'(t))$  and  $\mathbf{p}'(t)$ . Thus locating critical horizontal sections is equivalent to locating  $\pi$ -opening angle sections.

We have found that it is advantageous to further decompose the fundamental domain such that the curvature of its boundary curves have constant sign. To do that, we need to locate the boundary parameter where the curva-

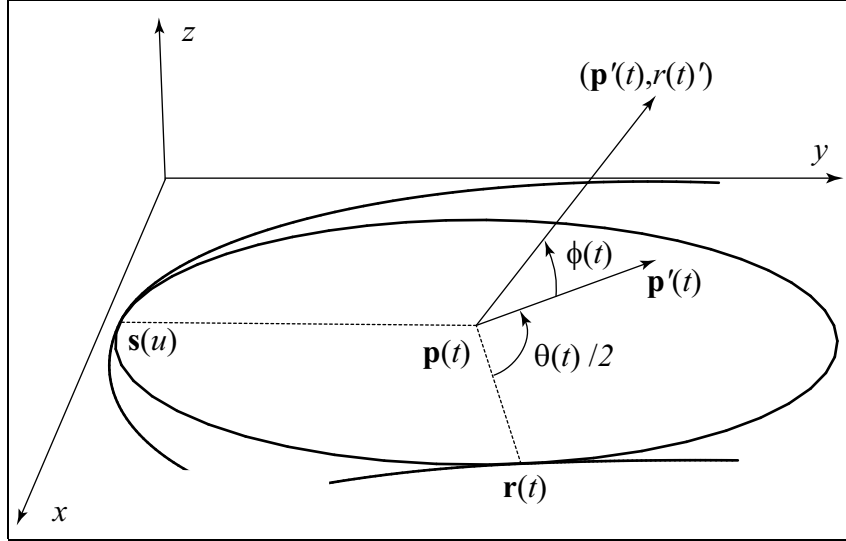


Figure 6: Opening angle

ture changes its sign. Candidates are those parameters where the curvature is discontinuous or zero.

The curvature  $\kappa(t)$  of a boundary curve  $\mathbf{r}(t)$  is defined by

$$\kappa(t) = \frac{\det(\mathbf{r}'(t), \mathbf{r}''(t))}{|\mathbf{r}'(t)|^{3/2}}. \quad (4)$$

According to this definition, a curve with positive (resp., negative) curvature will bend to the left (resp., right) as one is going along the curve in the direction of increasing  $t$ . See Figure 7.

For a rational  $\mathbf{r}(t) = (x(t)/w(t), y(t)/w(t))$ , we have

$$\kappa = \frac{w^3(x(y'w'' - y''w') + y(w'x'' - w''x') + w(x'y'' - x''y'))}{((xw' - x'w)^2 + (yw' - y'w)^2)^{3/2}} \quad (5)$$

Thus, if  $\mathbf{r}(t)$  is a rational curve of degree  $n$ , locating zero-curvature points of  $\mathbf{r}$  amounts to solving  $3n - 3$  order univariate polynomial equations ( $2n - 3$  if polynomial curve). At the zero-curvature points on the boundary, we can get the corresponding medial axis transform points. By these medial axis transform points, the original domain is further decomposed into fundamental domains whose boundary curves have constant curvature sign except possibly at the end points. We can classify these fundamental domains into four possible cases according to the curvature sign. For convenience' sake, we adopt the following conventions for the curvatures  $\kappa_{\mathbf{r}}$  and  $\kappa_{\mathbf{s}}$  of  $\mathbf{r}$  and  $\mathbf{s}$ , respectively: we denote  $\kappa_* > 0$  if  $\kappa_*(t) > 0$  for all  $t$  except possibly for  $t = 0, 1$

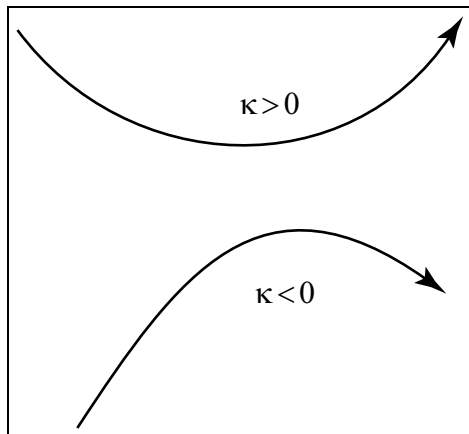


Figure 7: Curvature sign convention

and  $\kappa_* \geq 0$  if  $\kappa_* > 0$  or  $\kappa_*(t) \equiv 0$  for all  $t$ . Similarly  $\kappa_* < 0$  and  $\kappa_* \leq 0$  are defined.

Now we describe how to locate  $\pi$ -opening angle sections case by case.

**Case 1:  $\kappa_{\mathbf{r}} \leq 0$  and  $\kappa_{\mathbf{s}} \leq 0$**

For any given contact point  $\mathbf{r}(t)$  on  $\mathbf{r}$ , let  $\mathbf{s}(u)$  be the corresponding contact point of  $\mathbf{r}(t)$  on  $\mathbf{s}$ . Note that  $u = u(t)$  is a decreasing function of  $t$  due to the orientation convention of the boundary curve. Let  $\alpha(t)$  and  $\beta(u)$  be the angle of  $\mathbf{r}'(t)$  and  $\mathbf{s}'(u)$  with respect to the positive  $x$ -axis, respectively. Then we have

$$\theta(t) = \beta(u) - \alpha(t), \quad (6)$$

which means that the opening angle  $\theta(t)$  is equal to the angle from  $\mathbf{r}'(t)$  to  $\mathbf{s}'(u)$ . (See Figure 8.) Since  $\beta(u)$  is a decreasing function of  $u$  and  $u = u(t)$  and  $\alpha(t)$  are decreasing functions of  $t$ ,  $\theta(t)$  is increasing function of  $t$ .

From this observation we have the following result.

**Proposition 2.** *If  $\theta(0) > \pi$  or  $\theta(1) < \pi$ , there is no critical horizontal sections in  $\Omega_F$ . If  $\theta(0) \leq \pi$  and  $\theta(1) \geq \pi$ , there exists exactly one critical horizontal section, which is a valley in  $\Omega_F$ . In this case, if both  $\mathbf{r}$  and  $\mathbf{s}$  are line segments, i.e.,  $\kappa_{\mathbf{r}} \equiv 0$  and  $\kappa_{\mathbf{s}} \equiv 0$  then the whole  $\mathbf{MAT}(\Omega_F)$  is a critical horizontal section. Otherwise, the critical horizontal section is a single point.*

The location of this valley point can be approximated to any given tolerance by bisection method: Let  $\mathbf{r}(t)$  be a given point with  $0 < t < 1$ . Compute the intersection point of  $\mathbf{s}$  and the normal line of  $\mathbf{r}(t)$ . The angle  $\xi$  defined

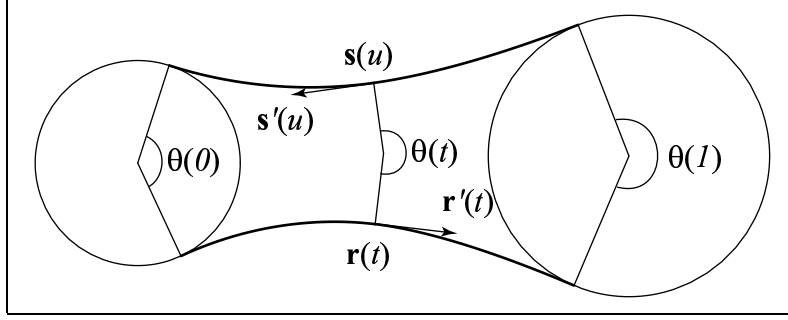


Figure 8:  $\kappa_{\mathbf{r}} \leq 0, \kappa_{\mathbf{s}} \leq 0$

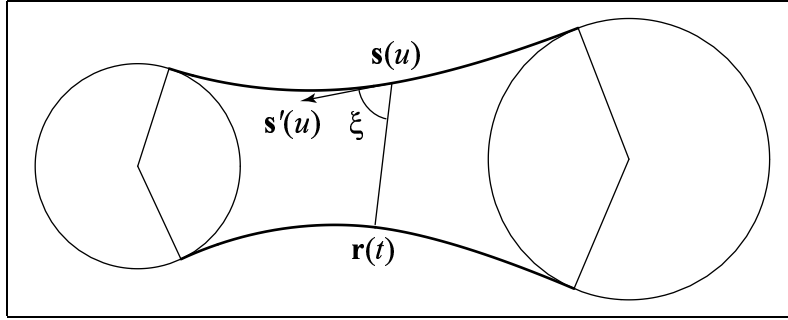


Figure 9: Valley locating process

by  $\mathbf{s}'(u)$  and  $\overrightarrow{\mathbf{s}(u)\mathbf{r}(t)}$  indicates which side of  $t$  the valley exists. That is, if  $\xi < \pi/2$  then the valley's contact point lies on  $\mathbf{r}(c)$  for some  $0 < c < t$  and if  $\xi > \pi/2$ , then for  $t < c < 1$ . Applying this process recursively, we can trap the valley in a sufficiently small region.

**Case 2:**  $\kappa_{\mathbf{r}} \geq 0, \kappa_{\mathbf{s}} \geq 0$

This case is analogous to the Case 1. Proposition 3.1 can be adapted as follows.

**Proposition 3.** *If  $\theta(0) < \pi$  or  $\theta(1) > \pi$ , there is no critical horizontal sections in  $\Omega_F$ . If  $\theta(0) \geq \pi$  and  $\theta(1) \leq \pi$ , there exists exactly one critical horizontal section, which is a peak in  $\Omega_F$ . In this case, if both  $\mathbf{r}$  and  $\mathbf{s}$  are line segments, i.e.,  $\kappa_{\mathbf{r}} \equiv 0$  and  $\kappa_{\mathbf{s}} \equiv 0$  then the whole  $\mathbf{MAT}(\Omega_F)$  is a critical horizontal section. Otherwise, the critical horizontal section is a single point.*

The locating algorithm is similar as in Case 1.

**Case 3:**  $\kappa_{\mathbf{r}} > 0, \kappa_{\mathbf{s}} < 0$

(By changing the roles of  $\mathbf{r}$  and  $\mathbf{s}$ , we can also cover the case  $\kappa_{\mathbf{r}} < 0, \kappa_{\mathbf{s}} > 0$ .)

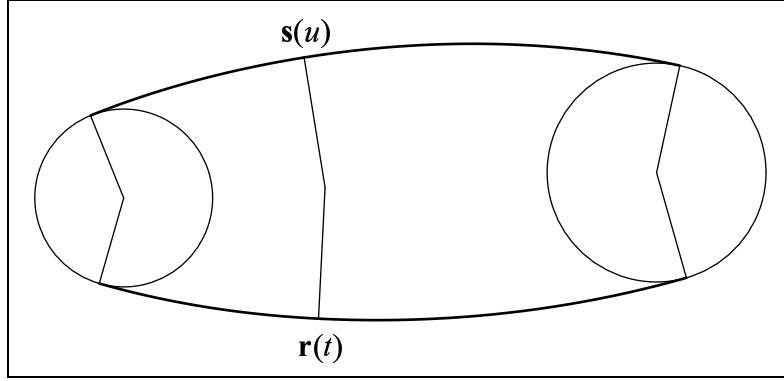


Figure 10:  $\kappa_{\mathbf{r}} \geq 0$ ,  $\kappa_{\mathbf{s}} \geq 0$

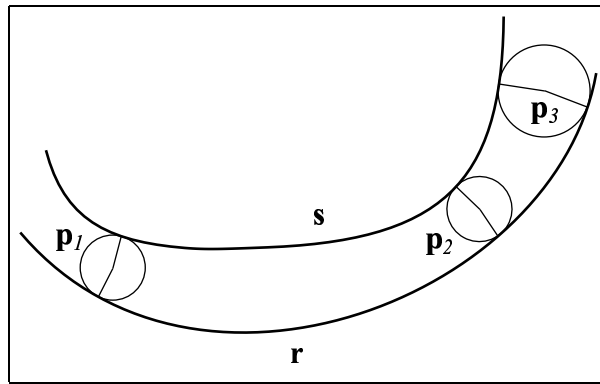


Figure 11:  $\kappa_{\mathbf{r}} > 0$ ,  $\kappa_{\mathbf{s}} < 0$

In this case we cannot tell the existence of peak or valley, or how many there are, if any, with only the data of  $\theta(0)$  and  $\theta(1)$ . In general, one can cook up an example which has as many peaks and valleys as one wishes with given  $\theta(0)$  and  $\theta(1)$  and under the condition  $\kappa_{\mathbf{r}} > 0$ ,  $\kappa_{\mathbf{s}} < 0$ . For example, in Figure 11 we have one peak and one valley between  $\mathbf{p}_1$  and  $\mathbf{p}_3$  whereas none of them between  $\mathbf{p}_2$  and  $\mathbf{p}_3$ . (Note that  $\mathbf{p}_1$  and  $\mathbf{p}_2$  have the same opening angle and radius.) Moreover, we cannot exclude the possibility that portions of  $\mathbf{r}$  and  $\mathbf{s}$  are offset curves to each other. We begin with this problem. Since  $\mathbf{MAT}(\Omega)$  is a real analytic curve at every generic 2-prong point and our fundamental domain consists of generic 2-prong only (except possibly at the end points),  $\mathbf{MAT}(\Omega_F)$  is a real analytic curve. By the real analyticity of radius component of  $\mathbf{MAT}(\Omega_F)$ , we have the following:

**Theorem 4.** *Either the whole  $\mathbf{MAT}(\Omega_F)$  is a  $c$ -horizontal section for some  $c > 0$ , or every  $c$ -horizontal section of  $\mathbf{MAT}(\Omega_F)$  consists of a finite number of points.*

That is, either the whole  $\mathbf{r}$  and  $\mathbf{s}$  are offset curves to each other (in this case we call  $\Omega_F$  a *parallel fundamental domain*), or there is a finite number of critical radius points. The decision whether or not  $\Omega_F$  is parallel can be made in finite steps. The criterion for this is given in Theorem 6. Bezout's theorem is crucial in proving this theorem.

**Theorem 5 (Bezout's Theorem).** *Two relatively prime polynomials  $f, g \in \mathbb{C}[x, y]$  of degree  $d_1$  and  $d_2$  can have at most  $d_1 d_2$  simultaneous solutions.*

For a given polynomial  $h(x, y)$ , the equation  $h(x, y) = 0$  usually defines a curve in  $\mathbb{R}^2$ . But in some cases, the solution of  $h(x, y) = 0$  consists of a single point. (For example  $h(x, y) = x^2 + y^2$ .) We call such a solution an isolated solution. To be precise, a point  $(x_0, y_0)$  is called an isolated solution of the equation  $h(x, y) = 0$ , if for some neighborhood  $V$  of  $(x_0, y_0)$ , there is no other solution than  $(x_0, y_0)$  in  $V$ .

The next is then an easy corollary of Bezout's theorem.

**Corollary.** *Let  $h(x, y)$  be an irreducible polynomial over  $\mathbb{R}$  of positive degree  $d$ . Then  $h(x, y) = 0$  can have at most  $d(d - 1)$  isolated solutions.*

*Proof.* If  $(x_0, y_0)$  is an isolated solution of  $h(x, y) = 0$ , then  $\frac{\partial h}{\partial x}(x_0, y_0) = \frac{\partial h}{\partial y}(x_0, y_0) = 0$ . That is,  $(x_0, y_0)$  is a simultaneous solution of

$$h(x, y) = 0 \tag{7}$$

$$\frac{\partial h}{\partial x}(x, y) = 0 \tag{8}$$

$$\frac{\partial h}{\partial y}(x, y) = 0. \tag{9}$$

Since  $h$  is irreducible,  $h$  and  $\frac{\partial h}{\partial x}$  (or  $\frac{\partial h}{\partial y}$ ) are relatively prime. Now the result follows from Bezout's theorem.  $\square$

**Theorem 6.** *Let  $\Omega_F$  be a fundamental domain with boundary curves  $\mathbf{r}$  and  $\mathbf{s}$ . Suppose  $\mathbf{r}$  and  $\mathbf{s}$  are rational curves of degree  $m$  and  $n$  respectively. Then  $\Omega_F$  is parallel if and only if:*

1.  $r(0) = r(1)$ , and
2. For some distinct  $N + 1$  points  $0 = t_0, \dots, t_N = 1$ , where  $N = (2m + 2n - 1)^2$ , we have  $\theta(t_0) = \dots = \theta(t_N) = \pi$ .

If  $\Omega_F$  is parallel, then for *any*  $N + 1$  points, the second condition is satisfied. What this theorem says is that any *one* set  $S$  of  $N + 1$  points is enough. If one of  $t_i$  in  $S$  does not satisfy the condition, then  $\Omega_F$  is not parallel. Otherwise, i.e., if every  $t_i$  in  $S$  does satisfy the condition, then  $\Omega_F$  is parallel.

*Proof.* One way is obvious. Conversely, let  $\mathbf{s}(u_i)$ ,  $i = 0, \dots, N$  be the corresponding contact points of  $\mathbf{r}(t_i)$  on  $\mathbf{s}$ . Since  $\theta(t_i) = \pi$ ,  $(t_i, u_i)$  are solutions of

$$\mathbf{r}'(t) \cdot (\mathbf{r}(t) - \mathbf{s}(u)) = 0 \quad (10)$$

$$\mathbf{s}'(u) \cdot (\mathbf{s}(u) - \mathbf{r}(t)) = 0. \quad (11)$$

If one substitutes

$$\mathbf{r}(t) = \frac{1}{c(t)}(a(t), b(t)) \quad (12)$$

$$\mathbf{s}(u) = \frac{1}{f(u)}(d(u), e(u)), \quad (13)$$

the above equations are reduced to polynomial equations

$$P(t, u) = (af - cd)(a'c - ac') + (bf - ce)(b'c - bc') = 0 \quad (14)$$

$$Q(t, u) = (af - cd)(d'f - df') + (bf - ce)(e'f - ef') = 0. \quad (15)$$

Note that both  $P$  and  $Q$  have total degree of at most  $2m + 2n - 1$ . In view of Bezout's theorem,  $P$  and  $Q$  must have a common factor of positive degree. Let  $h$  be the greatest common divisor of  $P$  and  $Q$ . Suppose  $h$  is written as a product

$$h = h_1 \cdots h_r \quad (16)$$

of irreducibles over  $\mathbb{R}$  of positive degree  $d_1, \dots, d_r$ . Now if we write  $P = P_1 h$  and  $Q = Q_1 h$ , then  $(t_i, u_i)$  are simultaneous solutions of

$$P_1(t, u) = 0 \quad (17)$$

$$Q_1(t, u) = 0 \quad (18)$$

or solutions of one of the equations

$$h_1 = 0$$

$$\vdots$$

$$h_r = 0.$$

Put  $d_0 = 2m + 2n - 1 - d$  where  $d = d_1 + \dots + d_r$ . Since  $P_1$  and  $Q_1$  are relatively prime polynomials of degree  $d_0$ , they have at most  $d_0^2$  solutions and each  $h_i$  has at most  $d_i(d_i - 1)$  isolated solutions. The number of all these solutions amount to  $d_0^2 + d_1(d_1 - 1) + \dots + d_r(d_r - 1) < (d_0 + \dots + d_r)^2 < N + 1$ .

Thus, at least one of  $(t_i, u_i)$  is the solution of  $h_j$  which is not isolated. That is, for some  $i, j$  we have  $h_j(t_i, u_i) = 0$  and one of the partial derivative, say  $\frac{\partial h_j}{\partial u}(t_i, u_i)$ , is not equal to zero. By the implicit function theorem, there is  $\phi \in C^1$  such that  $(t, \phi(t))$ , for some neighborhood of  $t_i$ , is the solution of  $h_j(t, u)$  and hence Equation (8) and (9). By the way,  $L(t, u) = (\mathbf{r}(t) - \mathbf{s}(u)) \cdot (\mathbf{r}(t) - \mathbf{s}(u))$  under the constraints of (8) and (9) measures the diameter of the contact disks. If we substitute  $u = \phi(t)$ , then it is easy to see that  $\frac{dL}{dt}(t, \phi(t)) = 0$  in a neighborhood of  $t_i$ , which means that  $\Omega_F$  contains a parallel fundamental domain. By theorem 3.3, the whole  $\Omega_F$  must be parallel.  $\square$

Now we continue to locate critical horizontal sections in Case 3. After going through the above test, we are left to locate the discrete critical horizontal sections in  $\Omega_F$  as stated in Theorem 4. To achieve this goal, we introduce a procedure that is incrementally securing regions that are free of any critical horizontal sections.

Let us continue to suppose  $\kappa_r > 0$  and  $\kappa_s < 0$  as in Case 3. Let  $\alpha(t)$  be the angle of  $\mathbf{r}'(t)$  and  $\beta(u)$  be that of  $\mathbf{s}'(u)$  as in the proof of Proposition 2. Assume also that total angle variations of  $\mathbf{r}'(t)$  and  $\mathbf{s}'(u)$  do not exceed  $\pi$ , i.e.,

$$\Delta\alpha = \int_0^1 \kappa_r(t) |\mathbf{r}'(t)| dt < \pi, \quad (19)$$

$$\Delta\beta = \int_0^1 \kappa_s(u) |\mathbf{s}'(u)| du > -\pi. \quad (20)$$

The reason behind this assumption is that we don't want to deal with too bent fundamental domains. And this assumption can be easily satisfied by inserting some contact disks, if necessary, in the fundamental domain concerned. Now we are ready to start the procedure. Take  $\mathbf{r}(t_1)$  for any  $0 < t_1 < 1$  and let  $\mathbf{s}(u_1)$  be the corresponding contact point on  $\mathbf{s}$ . Let  $\theta_1$  be the opening angle at  $\mathbf{r}(t_1)$ . Note that  $\mathbf{r}'(t)$  rotates positively and  $\mathbf{s}'(u)$  negatively as the corresponding parameters increase. Suppose first  $\theta_1 > \pi$ . Since  $\beta(u_1) = \alpha(t_1) + \theta_1$ , the parameter  $t_2$  such that  $\alpha(t_2) + \pi = \beta(u_1)$ , i.e., such that  $\mathbf{r}'(t_2)$  is parallel to  $\mathbf{s}'(u_1)$  satisfies  $t_2 > t_1$ . Then we can claim that

**Proposition 7.** *The fundamental domain defined by contact disks  $\mathbf{r}(t_1)$  and  $\mathbf{r}(t_2)$  has no critical horizontal sections.*

*Proof.* Let  $\mathbf{s}(u_2)$  be the corresponding contact point of  $\mathbf{r}(t_2)$ ,  $\mathbf{p}$  be a medial axis point in the fundamental domain, and  $\mathbf{r}(t)$  and  $\mathbf{s}(u)$  be the contact points of  $\mathbf{p}$ . To prove that  $\mathbf{p}$  is not a critical horizontal section, it is enough

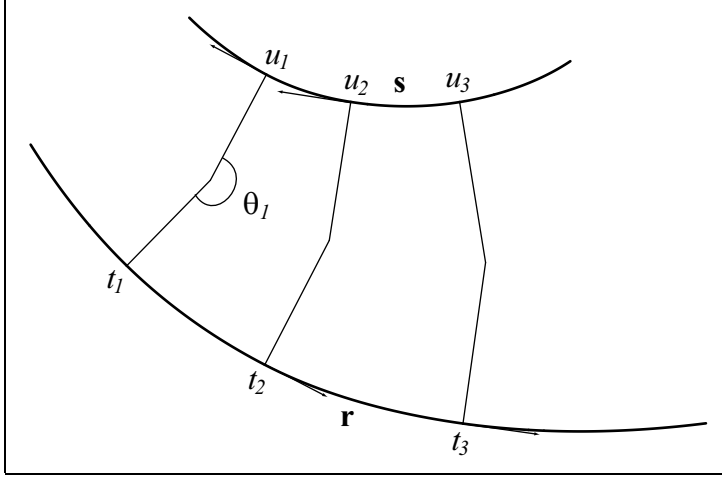


Figure 12: Monotone Region

to show that the opening angle of  $\mathbf{p}$ , i.e.,  $\beta(u) - \alpha(t)$  never equals  $2k\pi + \pi$  for any integer  $k$ . Note that we have  $t_1 < t < t_2$  and  $u_1 > u > u_2$ . Since  $\beta(u_1) < \beta(u) < \beta(u_2)$  and  $\alpha(t_1) < \alpha(t) < \alpha(t_2)$ , we have  $\beta(u_1) - \alpha(t_2) < \beta(u) - \alpha(t) < \beta(u_2) - \alpha(t_1)$ . Now the result follows by the observation that  $\beta(u_1) - \alpha(t_2) = \pi$  and  $\beta(u_2) - \alpha(t_1) = \beta(u_2) - \beta(u_1) + \theta_1 < \pi + \theta_1 < 3\pi$ .  $\square$

Now if  $\theta_1 < \pi$ , we have  $t_2 < t_1$  and the procedure follows similarly. Applying the above procedure recursively, we can obtain a sequence  $\{t_k\}$ .

**Theorem 8.** *If the sequence  $\{t_k\}$  converges to some  $0 \leq \tau \leq 1$ , then the medial axis transform point corresponding to  $\mathbf{r}(\tau)$  is a critical horizontal section.*

*Proof.* Since  $\alpha(t_k) + \theta_k = \beta(u_k)$  and  $\beta(u_k) - \alpha(t_{k+1}) = \pi$ , we have  $\alpha(t_{k+1}) - \alpha(t_k) = \theta_k - \pi$ . Furthermore, we have

$$\alpha(t_{k+1}) - \alpha(t_k) = \int_{t_k}^{t_{k+1}} \kappa_{\mathbf{r}}(t) |\mathbf{r}'(t)| dt.$$

Since  $\theta(t)$  is continuous and  $\theta(t_k) - \pi = \alpha(t_{k+1}) - \alpha(t_k)$ , we must have  $\theta(\tau) = \pi$ .  $\square$

Given any fundamental domain  $\Omega_F$  with  $\kappa_{\mathbf{r}} > 0$  and  $\kappa_{\mathbf{s}} < 0$ , we first take the medial axis transform point corresponding to the boundary point  $\mathbf{r}(\frac{1}{2})$ . From this medial axis transform point, we march (in both directions) to the nearest critical horizontal section in  $\Omega_F$ . If we are out of  $\Omega_F$  during the march, then  $\Omega_F$  has no critical horizontal section. Otherwise, if we come

to a critical horizontal section  $\mathbf{p}$ , we keep the record of  $\mathbf{p}$  and restart with the fundamental domain defined by  $\mathbf{p}$  and one of the medial axis transform points  $\mathbf{p}(0)$  and  $\mathbf{p}(1)$  that is closer to  $\mathbf{p}$ . In this way, we can locate all critical horizontal sections in  $\Omega_F$ .

## 4 Monotonic fundamental domain

Following the procedures of the previous sections, we can decompose the original domain into many fundamental domains containing no critical horizontal sections, i.e., no locally maximal or minimal radius component. Thus all of our fundamental domains have monotone increasing or decreasing radius function. We will call them *monotonic* fundamental domains.

Now we discuss the computation of offset curves in a monotonic fundamental domain  $\Omega_F$ . We can assume that a parameterization  $(\mathbf{p}(v), r(v))$  of  $\mathbf{MAT}(\Omega_F)$ , defined on the interval  $[0, 1]$ , so chosen that  $r(v)$  is monotone increasing. First of all, then, with the data of  $r(0)$  and  $r(1)$ , we can answer the question whether or not there exists any self-intersection points of the  $d$ -offset curves. Recall that the self-intersection points of  $d$ -offset curves are the medial axis points with a  $d$  radius value. We have also seen in [4] that  $d$ -offset curve is the envelope of  $d$ -cutoff of  $\mathbf{MAT}(\Omega_F)$ , where a  $d$ -cutoff of a subset  $A$  of  $\mathbb{R}_+^3 = \mathbb{R}^2 \times (\mathbb{R}^+ \cup \{0\})$  is defined by

$$A_d = \{(x, y, r) \in \mathbb{R}_+^3 \mid (x, y, r + d) \in A\}. \quad (21)$$

Now, if  $d < r(0)$ , there exists no self-intersection point since  $r(v) > d$  for all  $0 \leq u \leq 1$ . And the  $d$ -offset curves consist of pair of curves  $\mathbf{r}_d(t)$  and  $\mathbf{s}_d(u)$  for  $t, u \in [0, 1]$ . On the other hand, if  $r(0) \leq d \leq r(1)$ , then  $r(v) = d$  for exactly one  $v \in [0, 1]$ . (Unless  $r(0) = r(1)$ , i.e.,  $\Omega_F$  is a parallel fundamental domain. In this case, the  $d$ -offset curve is  $\mathbf{MA}(\Omega_F)$  itself.) Finally, if  $r(1) < d$ , then the  $d$ -cutoff of  $\mathbf{MAT}(\Omega_F)$  is an empty set, which means that there is no  $d$ -offset curve at all in  $\Omega_F$ . We summarize these results as follows (see also Figure 13,14, and 15):

- $d < r(0)$ : Since  $r(v) > d$  for all  $v \in [0, 1]$ ,  $(p(v), r(v) - d)$  is a parameterization of  $\mathbf{MAT}(\Omega_F)_d$  for  $v \in [0, 1]$  and there is no self-intersection points.
- $r(0) \leq d \leq r(1)$ : Since  $r(v)$  is monotonic increasing, there exists unique  $c \in [0, 1]$  satisfying  $r(c) = d$ . Then  $(p(v), r(v) - d)$  for  $c \leq u \leq 1$  is a parameterization of  $\mathbf{MAT}(\Omega_F)_d$  and  $\mathbf{p}(c)$  is the self-intersection point.
- $r(1) < d$ : Since  $r(v) < d$  for all  $v \in [0, 1]$ ,  $\mathbf{MAT}(\Omega_F)_d$  is empty, and so is the  $d$ -offset curve.

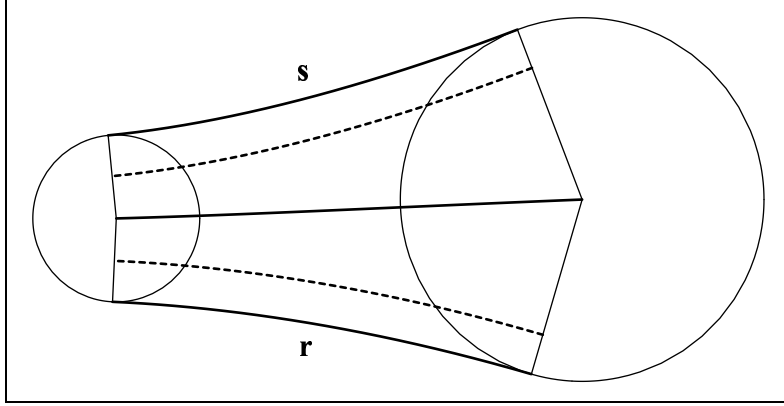


Figure 13:  $d < r(0) \leq r(1)$

So, as we go through each monotonic fundamental domain  $\Omega_F$ , one by one, of the original domain  $\Omega$ , we do nothing and just ignore it if  $d > r(0)$  and  $d > r(1)$ . If  $d < r(0)$  and  $d < r(1)$ , we compute  $\mathbf{r}_d$  and  $\mathbf{s}_d$  and record them as  $d$ -offset curve of  $\Omega_F$ . Finally, if  $r(0) \leq d \leq r(1)$  or  $r(0) \geq d \geq r(1)$ , we first check if  $\Omega_F$  is parallel. If so,  $\mathbf{r}_d$ ,  $\mathbf{s}_d$ , and  $\mathbf{MA}(\Omega_F)$  are all the same and each of them is the  $d$ -offset curve of  $\Omega_F$ . If  $\Omega_F$  is not parallel, the unique self-intersection point can be located as follows. We can consider that  $\mathbf{MAT}(\Omega_F)$  is parameterized by  $t$  or  $u$ , the parameters of the boundary curve  $\mathbf{r}$  or  $\mathbf{s}$ , respectively. The fact that we can get the medial axis transform point  $(\mathbf{p}(t), r(t))$  for any given boundary point  $\mathbf{r}(t)$  for  $t \in [0, 1]$  amounts to that we can “evaluate” the  $\mathbf{MAT}(\Omega_F)$  as a function of  $t$ , especially the radius component  $r(t)$ . Recall that the self-intersection point is equivalent to solution of  $r(t) = d$ . Thus we can apply any numerical approximation scheme to solve this equation, for example the Newton-Raphson method. (Note that we can evaluate the derivative  $r'(t)$  by the relation 3.) After we find the self-intersection point, or equivalently the contact disk with radius  $d$ , the fundamental domain  $\Omega_F$  is divided by the contact disk. The resulting two fundamental domains are just those considered above and we treat them accordingly.

## 5 Error analysis

In fact, what we have done so far is to specify parameter intervals of the boundary curve  $\mathbf{r}(t)$  such that  $\mathbf{r}_d(t)$  on those intervals are the  $d$ -offset curve of the boundary. To complete the whole work, one need approximate  $\mathbf{r}_d(t)$  on each interval. As we have pointed out in the introduction, the approximation

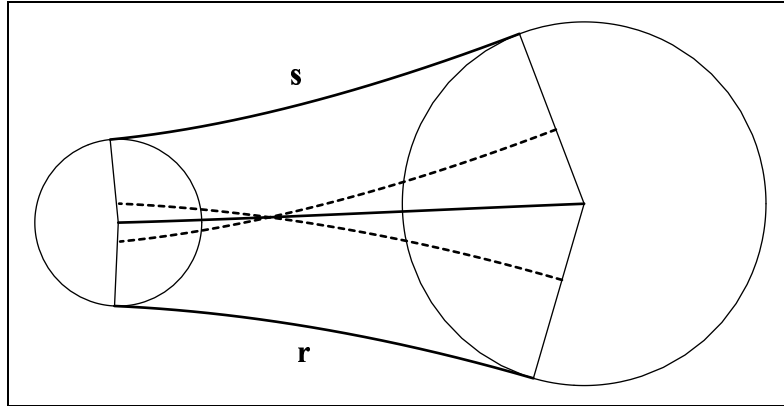


Figure 14:  $r(0) \leq d \leq r(1)$

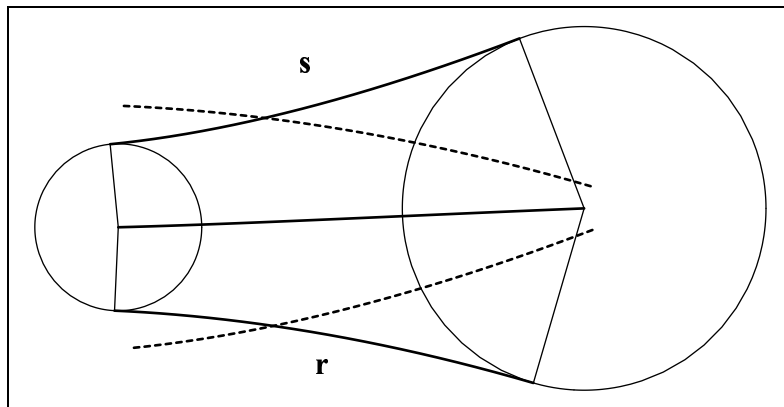


Figure 15:  $r(0) \leq r(1) < d$

of  $\mathbf{r}_d(t)$  is unavoidable due to the irrational term in Equation (1). Of course, if  $\mathbf{r}(t)$  is a Pythagorean hodograph curve, then the irrational term disappears and  $\mathbf{r}_d(t)$  can be represented by an exact rational curve.

There are a lot of literature dealing with approximation of  $\mathbf{r}_d(t)$  from  $\mathbf{r}(t)$  in the given interval, and we do not address any new approximation method here. Instead we are going to discuss how to compute error of  $\mathbf{r}_d(t)$ . If the computed error is beyond the given tolerance, we have to subdivide the interval to increase the precision of approximation.

Let  $\mathbf{w}(s)$  be an approximation of  $\mathbf{r}_d(t)$ . We may suppose that  $\mathbf{w}(s)$  and  $\mathbf{r}(t)$  are defined on the unit interval  $[0, 1]$ . Then the error is defined by

$$E(s, t) = |\mathbf{w}(s) - \mathbf{r}(t)| - d,$$

where  $s$  and  $t$  must satisfy the constraint

$$F(s, t) = (\mathbf{w}(s) - \mathbf{r}(t)) \cdot \mathbf{r}'(t) = 0.$$

That is, for a given point  $\mathbf{r}(t)$ , we measure the length  $\overline{\mathbf{w}(s)\mathbf{r}(t)}$  such that  $\overline{\mathbf{w}(s)\mathbf{r}(t)}$  is normal to the tangent of  $\mathbf{r}(t)$ , and see how much it deviates from  $d$ . Of course, if  $\mathbf{w}$  is true  $d$ -offset curve, then  $E \equiv 0$ .

The extreme points of  $E(s, t)$ , constrained by  $F(s, t) = 0$ , are among the critical points of the function  $H$

$$H(s, t, \lambda) = E(s, t) + \lambda F(s, t).$$

The critical points of  $H$  are the solutions of the equations

$$0 = \frac{\partial H}{\partial s} = \frac{\partial E}{\partial s} + \lambda \frac{\partial F}{\partial s} \quad (22)$$

$$0 = \frac{\partial H}{\partial t} = \frac{\partial E}{\partial t} + \lambda \frac{\partial F}{\partial t} \quad (23)$$

$$0 = \frac{\partial H}{\partial \lambda} = F(s, t), \quad (24)$$

where

$$\begin{aligned} \frac{\partial E}{\partial s} + \lambda \frac{\partial F}{\partial s} &= \left( \frac{\mathbf{w}(s) - \mathbf{r}(t)}{|\mathbf{w}(s) - \mathbf{r}(t)|} + \lambda \mathbf{r}'(t) \right) \cdot \mathbf{w}'(s) \\ \frac{\partial E}{\partial t} + \lambda \frac{\partial F}{\partial t} &= -\frac{\mathbf{w}(s) - \mathbf{r}(t)}{|\mathbf{w}(s) - \mathbf{r}(t)|} \cdot \mathbf{r}'(t) - \\ &\quad \lambda (|\mathbf{r}'(t)|^2 - (\mathbf{w}(s) - \mathbf{r}(t)) \cdot \mathbf{r}''(t)). \end{aligned}$$

Then Equation (24) reduces Equation (23) to

$$\lambda (|\mathbf{r}'(t)|^2 - (\mathbf{w}(s) - \mathbf{r}(t)) \cdot \mathbf{r}''(t)) = 0. \quad (25)$$

Now, if  $\lambda = 0$ , Equation (22) becomes

$$(\mathbf{w}(s) - \mathbf{r}(t)) \cdot \mathbf{w}'(s) = 0, \quad (26)$$

that is,  $\overline{\mathbf{w}(s)\mathbf{r}(t)}$  is normal to the tangent of  $\mathbf{w}(s)$ . And if  $\lambda \neq 0$ , Equation (24) and (25) generate

$$\mathbf{w}(s) - \mathbf{r}(t) = m \frac{\mathbf{r}'(t)}{|\mathbf{r}'(t)|} \times \mathbf{z}, \quad (27)$$

where  $\mathbf{z}$  is the unit normal vector to the plane and

$$m = -\frac{|\mathbf{r}'(t)|^3}{(\mathbf{r}'(t) \times \mathbf{r}''(t)) \cdot \mathbf{z}}.$$

One can easily check that  $\mathbf{w}(s)$  of Equation (27) coincides the center of curvature of  $\mathbf{r}(t)$ .

Now, to identify extreme points of  $E$ , i.e, to find the maximal deviation of  $|\overline{\mathbf{w}(s)\mathbf{r}(t)}|$  from  $d$ , we increment  $t$  from 0 to 1 in step  $\Delta t$ , and find the intersection point  $\mathbf{w}(s)$  of the normal line of  $\mathbf{r}(t)$  and  $\mathbf{w}$ . Then we calculate

$$\begin{aligned} & \cos \phi, \\ & (\mathbf{w}(s) - \mathbf{r}(t)) \cdot \mathbf{r}''(t) - |\mathbf{r}'(t)|^2, \end{aligned}$$

where  $\phi$  is the angle between  $\overline{\mathbf{w}(s)\mathbf{r}(t)}$  and  $\mathbf{w}'(s)$ . If any of these quantities change their signs between successive  $t$ , say  $k\Delta t$  and  $(k+1)\Delta t$ , they indicates the existence of a maximal deviation in the interval  $[k\Delta t, (k+1)\Delta t]$ . By recursively applying the above procedure to the interval  $[k\Delta t, (k+1)\Delta t]$ , we can locate the parameter  $t$  where the maximal deviation occurs. If the error is beyond the given tolerance, we have to insert a contact disk at  $\mathbf{r}(t)$  and reduce the error until the tolerance is satisfied.

## 6 Illustrative example

In Figure 16, a domain with a hole inside is decomposed into three fundamental domains. This process was addressed in [5]. In Figure 17, we inserted three contact disks that correspond to the inflection points of the boundary curve. Now the resulting fundamental domains' boundaries have constant curvature signs. In Figure 18, all peaks and valleys are found, if any, in each fundamental domain. Now the resulting fundamental domains are monotonic fundamental domains. In Figure 19, the self-intersection points for a given value  $d$  are found, if any, in each monotonic fundamental domain. Finally in Figure 20, offset curves are computed in each valid fundamental domain.

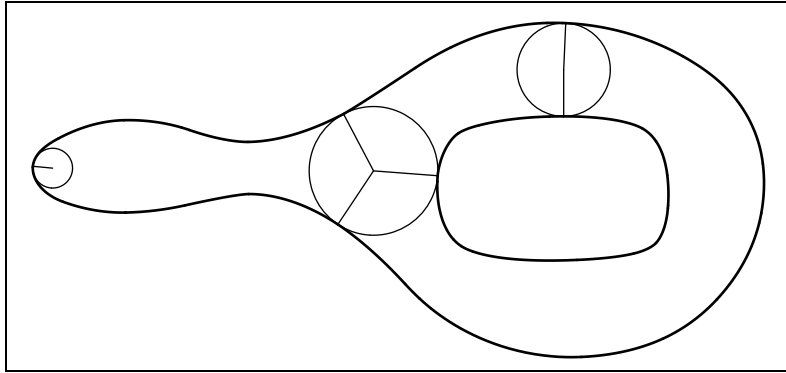


Figure 16: step 1

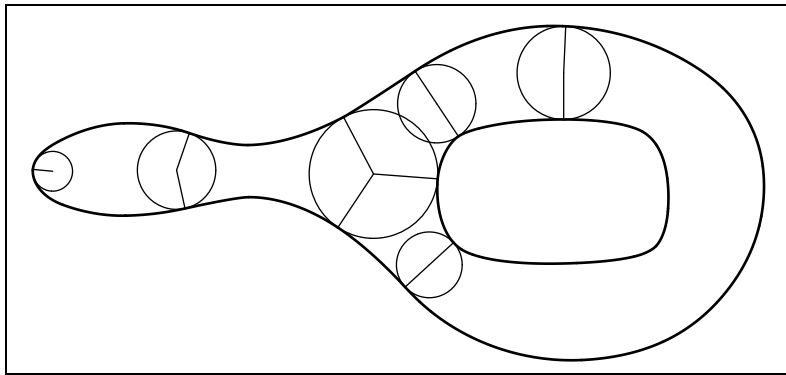


Figure 17: step 2

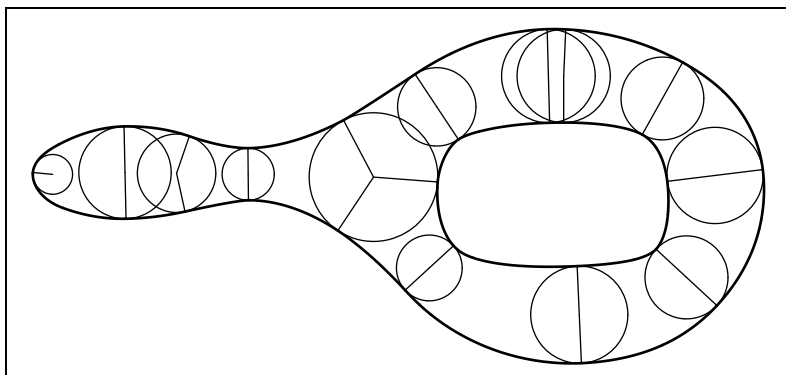


Figure 18: step 3

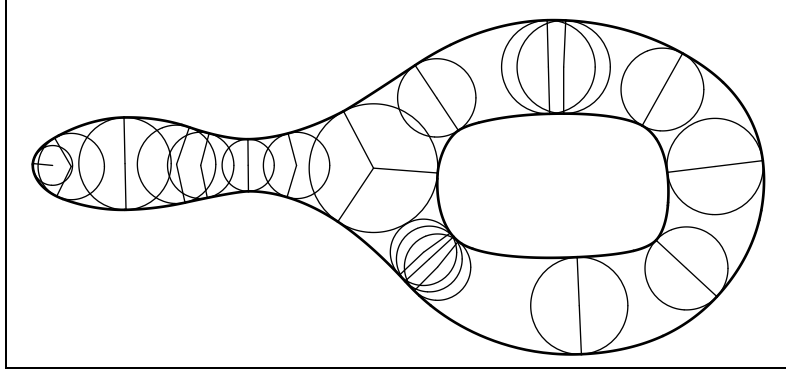


Figure 19: step 4

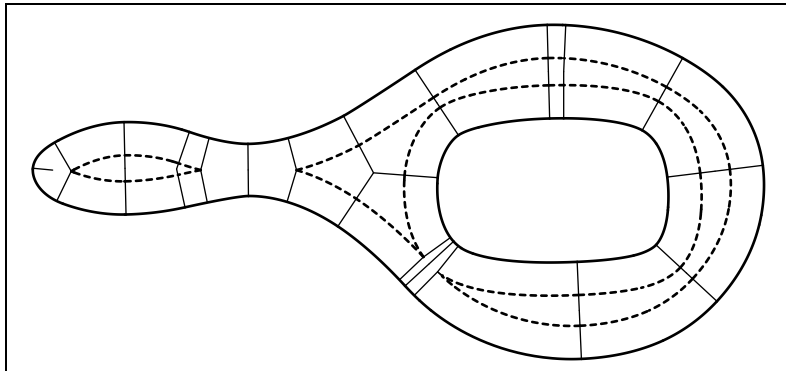


Figure 20: step 5

## References

- [1] H. Blum. A Transformation for Extracting New Descriptors of Shape. In W. W. Dunn, editor, *Proc. Symp. Models for the Perception of Speech and Visual Form*, pages 362–380. MIT Press, Cambridge, MA, USA, 1967.
- [2] C.-S. Chiang, C. M. Hoffmann, and R. E. Lynch. How to compute offsets without self-intersection. Technical Report CSD-TR-91-072, Computer Sciences Department, Purdue University, October 1991.
- [3] H. I. Choi, S. W. Choi, C. Y. Han, H. P. Moon, K. H. Roh, and N.-S. Wee. Two-dimensional offsets via medial axis transform I: Mathematical theory. in preparation, 1999.
- [4] H. I. Choi, S. W. Choi, and H. P. Moon. Mathematical theory of medial axis tranform. *Pacific Journal of Mathematics*, 181(1):57–88, 1997.
- [5] H. I. Choi, S. W. Choi, H. P. Moon, and N.-S. Wee. New algorithm for medial axis transform of plane domain. *Graphical Models and Image Processing*, 59(6):463–483, November 1997.
- [6] J. J. Chou and E. Cohen. Computing offsets and tool paths with Voronoi diagrams. Technical Report UUCS-89-017, Department of Computer Science, University of Utah, Salt Lake City, UT 84112 USA, August 1990.
- [7] R. Farouki. Pythagorean-hodograph curves in practical use. In R. Barnhill, editor, *Geometry Processing for Design and Manufacturing*, pages 3–33. SIAM, Philadelphia, 1992.
- [8] R. Farouki and T. Sakkalis. Pythagorean-hodograph space curves. *Advances in Computational Mathematics*, 2:41–66, 1994.
- [9] R. T. Farouki and J. K. Johnstone. The bisector of a point and a plane parametric curve. *Computer Aided Geometric Design*, 11:117–151, 1994.
- [10] R. T. Farouki and J. K. Johnstone. Computing point/curve and curve/curve bisectors. In R. B. Fisher, editor, *Design and Application of Curves and Surfaces*, pages 327–354. Oxford University Press, 1994.
- [11] R. T. Farouki and C. A. Neff. Algebraic properties of plane offset curves. *Computer Aided Geometric Design*, 7:101–127, 1990.

- [12] R. T. Farouki and C. A. Neff. Analytic properties of plane offset curves. *Computer Aided Geometric Design*, 7:83–99, 1990.
- [13] R. T. Farouki and C. A. Neff. Hermite interpolation by Pythagorean-hodograph quintics. *Mathematics of Computation*, 64:1589–1609, 1995.
- [14] R. T. Farouki and R. Ramamurthy. Specified-precision computation of curve/curve bisector. Technical Report UM-MEAM-96-10, Dept. of Mechanical Engineering and Applied Mechanics, University of Michigan, Ann Arbor, MI 48109.
- [15] R. T. Farouki and T. Sakkalis. Pythagorean hodographs. Technical Report RC15223, IBM Research, September 1990.
- [16] R. T. Farouki and T. W. Sederberg. Analysis of the offset to a parabola. *Computer Aided Geometric Design*, 12:639–645, 1995.
- [17] M. Held. *On the Computational Geometry of Pocket Machining*. Lecture Notes in Computer Science 500. Springer-Verlag, 1991.
- [18] M. Held, G. Lukács, and L. Andor. Pocket machining based on contour-parallel tool paths generated by means of proximity maps. *Computer-Aided Design*, 26(3):189–203, March 1994.
- [19] J. Hoschek. Offset curves in the plane. *Computer-Aided Design*, 17(2):77–82, March 1985.
- [20] J. Hoschek. Spline approximation of offset curves. *Computer Aided Geometric Design*, 5:33–40, 1988.
- [21] J. Hoschek and N. Wissel. Optimal approximate conversion of spline curves and spline approximation of offset curves. *Computer-Aided Design*, 20(8):475–483, October 1988.
- [22] R. Klass. An offset spline approximation for plane cubic splines. *Computer-Aided Design*, 15(5):297–299, September 1983.
- [23] D. T. Lee. Medial Axis Transform of a Planar Shape. *IEEE Trans. Pattern Analysis and Machine Intelligence*, PAMI-4(4):363–369, July 1982.
- [24] I.-K. Lee, M.-S. Kim, and G. Elber. Planar curve offset based on circle approximation. *Computer-Aided Design*, 28(8):617–630, 1996.

- [25] H. Persson. NC machining of arbitrarily shaped pockets. *Computer-Aided Design*, 10(3):169–174, May 1978.
- [26] M. Peternell and H. Pottmann. Applications of Laguerre Geometry in CAGD I,II. Technical Report 30,31, Institut für Geometrie, Technische Universität Wien, May 1996.
- [27] B. Pham. Offset approximation of uniform B-splines. *Computer-Aided Design*, 20(8):471–474, October 1988.
- [28] H. Pottmann. Curve design with rational Pythagorean-hodograph curves. *Advances in Computational Mathematics*, 3:147–170, 1995.
- [29] H. Pottmann. Rational curves and surfaces with rational offsets. *Computer Aided Geometric Design*, 12:175–192, 1995.
- [30] F. P. Preparata. The medial axis of a simple polygon. *Lecture Notes in Computer Science: Mathematical Foundation of Computer Science*, pages 443–450, 1977.
- [31] W. Tiller and E. G. Hanson. Offsets of two-dimensional profiles. *IEEE Computer Graphics and Applications*, pages 36–46, September 1984.
- [32] F.-E. Wolter. Cut Locus and Medial Axis in Global Shape Interrogation and Representation. *MIT Ocean Eng. Design Lab. memorandum*, 92(2), January 1992.